JAST, Vol. 3, No. 4, pp 195–204

JAST
Journal of Aerospace Science and Technology

Multi Fracture/Delamination Analysis of Composites Subjected to Impact Loadings

S. Mohammadi[1], A.A. Moosavi Khandan[2]

A combined finite/ discrete element method is presented for modelling composite specimens subjected to dynamic/impact loadings. The main task is set on developing an algorithm for simulation of potential bonding and debonding/delamination phenomena during impact or general dynamic loading conditions. In addition, full fracture analysis also be performed. The proposed approach adopts a general node to face nonlinear frictional contact algorithm to enforce bonding/debonding constraints between composite plies. The method is also capable of analyzing progressive fracture and fragmentation behaviour as well as potential post cracking interactions caused by the newly created crack sides and segments. A local remeshing technique is adopted every time a new crack is formed, while an overall remeshing is performed anytime a certain criterion of error estimation is violated. The special local remeshing technique is designed to geometrically model an individual crack by splitting the element, separating the failed node, creating new nodes and dividing the neighboring elements to preserve the compatibility conditions. The same procedure is capable of modelling application of fibre reinforced polymer (FRP) layers to other engineering structures in order to improve their flexible behavior in static and dynamic loading conditions.

INTRODUCTION

Composite structures are subject to various types of damage in their life time, induced by either chemical processes due to aggressive environmental conditions or loads higher than the design service loads. Progressive and catastrophic crack propagation is known to be a major safety concern in all composite applications. As a result, development of reliable and efficient models for determining failure behaviour of composites has been an active subject of computational research. One of the most considerable problems in designing composite structures is their vulnerability to transverse impact, which can cause significant internal damage in terms of delamination (debonding), matrix cracking, local and global bucklings and fragmentation.

For a wide range of composite applications, continuum mechanics has been frequently used to formulate the basic governing equations [1]. Their main disadvantage, however, has been in their restriction to laminates with simple geometries and behavior. More sophisticated models have been developed by adopting contact interaction algorithms within a finite element procedure for simulation of debonding behavior [2-7].

Nevertheless, the finite element method (FEM) has roots in the concepts of continuum mechanics, and is not suited to general crack propagation and in particular to fragmentation problems. In contrast, the recently revived discrete element method (DEM) is well suited to problems with strong material and geometric discontinuities [8].

This paper is dedicated to the introduction of a new approach based on the combined finite/discrete element method to fracture and delamination analysis of composites. The proposed algorithm consists of full material and geometric non-linearities. A central difference explicit time integration technique is adopted which is computationally efficient for impact simulations. The present discrete element method utilizes principles of penalty based contact mechanics in order to enforce developing contact constraints. The discrete element method can be basically regarded as a finite

1. *Associate Professor, Dept. of Civil Eng., Univ. of Tehran, Tehran, Iran, Email: smoham@ut.ac.ir.*
2. *Aerospace Engineer, MSC., Dept. of Civil Eng., Univ. of Tehran, Tehran, Iran.*

element method coupled with concepts of multi-body dynamics, specifically designed to solve problems that exhibit strong discontinuities [8].

First, the simulation strategy is briefly explained. Consider a composite plate is subjected to a high velocity impact by an external object as illustrated in Figure 1. The specimen is discretized by a finite element mesh, except for the potentially susceptible damage region of composite, which is modelled using discrete element mesh. Coarser finite elements may be used in regions far from the impact point and the potential damage region in order to reduce the analysis time. Each discrete element is discretized by a finite element mesh. Interlaminar characteristics of plies such as debonding, impenetrability, friction and sliding determine connection (bonding) states of the adjacent discrete elements. Plies bonding (debonding) interaction and the interlaminar behavior in the post delamination phase, such as slipping and crack faces interactions are governed by contact mechanics. Discrete element system and finite element mesh of the rest of the plate are connected together by transition interface, preventing separation/penetration under all stress conditions.

WEAK FORMULATION OF FEM WITH CONTACT MECHANICS

A weak form of the boundary value problem of the finite element formulation is adopted. Assume Ω and Γ represent the body of interest and its boundary, respectively. Also, the boundary is assumed to consist of a part with prescribed displacement u, Γ_u, a part with prescribed traction force f^{surf}, Γ_σ, and a part Γ_C in contact with another body (see Figure 2).

The variational form of the dynamic initial/boundary value problem can be expressed as [4]:

$$w^{\text{int}}(\delta u, u) + M(\delta u, u) = w^{ext}(\delta u) + w^{con}(\delta u) \tag{1}$$

where

$$w^{\text{int}}(\delta u, u) = \int_\Omega \delta(u) : (u) dv \tag{2}$$

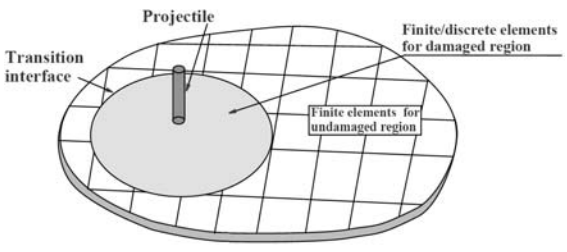

Figure 1. A composite plate subjected to a high velocity projectile. The combined finite element mesh is only used for the delaminated/fractured part. Damaged and undamaged regions are connected to each other by means of contact transition interfaces.

$$M(\delta u, u) = \int \delta u \cdot \rho \ddot{u} dv \tag{3}$$

$$w^{ext}(\delta u) = \int_\Omega \delta u \cdot f^{body} dv + \int_{\Gamma_u} \delta u \cdot f^{surf} da \tag{4}$$

$$w^{con}(\delta u) = \int_{\Gamma_c} \delta g(u) \cdot f^{con} da \tag{5}$$

denote, respectively, the virtual work of internal forces, the inertial forces contribution, the virtual work of external forces and the virtual work of contact forces. Here ó is the Cauchy stress tensor, å is the strain tensor, u is the displacement vector, while g represents the contact gap vector:

$$g = [g_N, g_T]^T \tag{6}$$

where g_N is the normal distance between contactor node and contact segment. g_T is a tangential vector whose size is equal to the distance between the projection of the contact node in the current configuration and the initial configuration. Figure 3 defines the adopted 3D node to face contact interaction model.

According to the weak form of the boundary value problem (1), the component form of the virtual work of the contact forces associated with the contact node is given by [4]:

$$\delta w^c = f_l^c \delta g_l = f_l^c \frac{\delta g_l}{\delta u_i^s} \delta u_i^s \tag{7}$$

where $l = n, t$ and $i = x, y$, and u_i^s is the i-component of the displacement vector at node s, and f^c is the contact force vector over the contact area A^c,

$$f^c = A^c \sigma^c \tag{8}$$

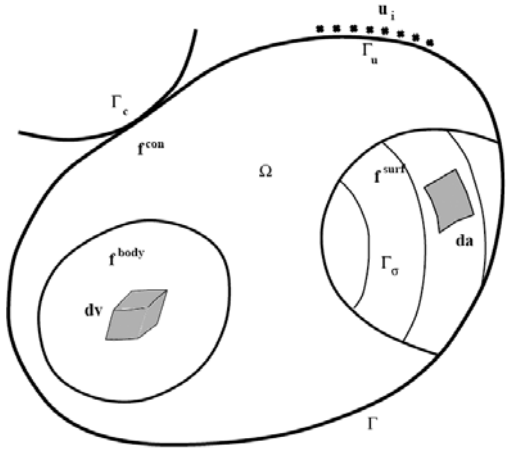

Figure 2. Boundary value problem for a body in contact with another body [8].

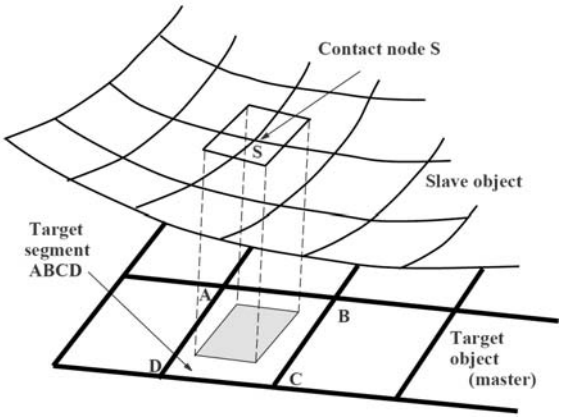

Figure 3. 3D node to face contact interaction.

$$\sigma = k^c g = \begin{bmatrix} k_n^c & 0 \\ 0 & k_t^c \end{bmatrix} \begin{bmatrix} g_n \\ g_t \end{bmatrix} \tag{9}$$

where k^c is the penalty term matrix , which may vary between contact nodes. The calculated contact force has to be distributed over the target and the contactor nodes [8].

INTERFACE MODEL

One of the major failure modes of composites subjected to impact loadings is the debonding failure in interface of composite plies. Here, a 3D Hashin model is adopted to predict initiation of interfacial debonding. Within a large deformation framework, the rate of Green-Lagrange strain tensor $\overline{\dot{E}}$ can be decomposed into elastic $\overline{\dot{E}}^{el}$ and inelastic $\overline{\dot{E}}^{in}$ parts.

$$\overline{\dot{E}} = \overline{\dot{E}}^{el} + \overline{\dot{E}}^{in} \tag{10}$$

$$\overline{\dot{E}}^{el} = \overline{C}\overline{\dot{S}} \tag{11}$$

where $\overline{C}$ is the elasticity matrix for plane isotropic behavior of the material and $\overline{S}$ is the stress matrix The inelastic strain rate follows the associated flow rule:[5-6]

$$\overline{\dot{E}}^{in} = \overline{\dot{E}}^{pl} = \dot{\lambda}\frac{\partial F}{\partial \overline{S}} \tag{12}$$

Here, λ is the inelastic coefficient and F is the yield function. The Hashin delamination criterion is defined as:

$$\frac{\left(\overline{S}^{33}\right)^2}{Z_\circ^2} + \frac{\left(\overline{S}^{13}\right)^2 + \left(\overline{S}^{23}\right)^2}{R_\circ^2} \leq 1 \tag{13}$$

where $\overline{S}^{33}$, $\overline{S}^{13}$, $\overline{S}^{23}$ are interlaminar stresses, and Z_0 and R_0 are tensile and tangential strengths of layer, respectively.

The yield function $F(\overline{S}, \beta)$ is defined from the delamination criterion and a linear softening function $Z(\beta)$:

$$F\left(\overline{S}, \beta\right) = g\left(\overline{S}\right) - Z\left(\beta\right) \leq 0 \tag{14}$$

$$g\left(\overline{S}\right) = \sqrt{\overline{S}^T A \overline{S}} \tag{15}$$

$$A = \begin{bmatrix} 0 & 0 & 0 & 0 & 0 & 0 \\ 0 & 0 & 0 & 0 & 0 & 0 \\ 0 & 0 & 1 & 0 & 0 & 0 \\ 0 & 0 & 0 & 0 & 0 & 0 \\ 0 & 0 & 0 & 0 & \left(\frac{Z_\circ}{R_\circ}\right)^2 & 0 \\ 0 & 0 & 0 & 0 & 0 & \left(\frac{Z_\circ}{R_\circ}\right)^2 \end{bmatrix} \tag{16}$$

$$Z\left(\beta\right) = Z_\circ\left(1 - \mu\beta\right) \tag{17}$$

The internal variable β can be assumed as the equivalent inelastic strain. The parameter μ describes the slope of the softening function $Z(\beta)$. It is a material parameter and can be determined from the critical energy release rate G_c, tensile strength Z_0 and the thickness of the intermediate layer h_T:

$$\mu = \frac{Z_\circ \times h_T}{2G_c} \tag{18}$$

The rate of the internal variable β is defined from the evolution law:

$$\dot{\beta} = -\dot{\lambda}\frac{\partial F}{\partial Z} \tag{19}$$

The gradient of the yield function F is derived as follows:[9]

$$\frac{\partial F}{\partial \overline{S}} = \frac{1}{g\left(\overline{s}\right)} A\overline{S} = N \tag{20}$$

$$\frac{\partial F}{\partial Z} = -1 \tag{21}$$

Adopting a backward Euler algorithm within a time step $t_{n+1} = t_n + \Delta t$, and using equations (10-12) yields to:

$$\overline{E}_{n+1} = \overline{C}^{-1}\overline{S}_{n+1} + \overline{E}_n^{pl} + \frac{\lambda}{g\left(\overline{S}_{n+1}\right)} A\overline{S}_{n+1} \tag{22}$$

$$\overline{S}_{n+1} = \left[\overline{C}^{-1} + \frac{\lambda}{Z\left(\beta_{n+1}\right)} A\right]\left[\overline{E}_{n+1} - \overline{E}_n^{pl}\right] \tag{23}$$

$$\overline{S}_{n+1} = P\overline{E}^{tr} \tag{24}$$

where subscripts $_n$ and $_{n+1}$ are associated with times t_n and t_{n+1}, respectively. Updating the internal parameter β is performed using a backward Euler integration:

$$\beta_{n+1} = \beta_n + \lambda \tag{25}$$

Linearization of the stress tensor has to be derived for the finite element formulation. After some algebraic manipulations, the consistent tangent matrix can be derived:

$$\overline{D} = P - \frac{PN\,(PN)^T}{N^T PN + H} \tag{26}$$

$$H = \frac{Z'}{1 - \lambda \frac{Z'}{Z}} \tag{27}$$

$$Z' = -\mu \tag{28}$$

HOFFMANN MATERIAL MODEL

The behaviour of the composite material is assumed to follow the anisotropic Hoffmann model. It requires six normal tensile $\overline{\sigma}_T$ and compressive $\overline{\sigma}_C$ strengths in three orthogonal directions and three shear strengths $\overline{\sigma}_S$. The imminence of material failure by the orthotropic Hoffman criterion is defined by [10]

$$\Phi = \frac{1}{2}\sigma^T \mathrm{P}\sigma + \sigma^T \mathrm{p} - \overline{\sigma}^2(\kappa) \tag{29}$$

where the projection vector p and the projection matrix P are defined based on nine material yield strengths, a normalized yield strength $\overline{\sigma}$, and a softening/hardening parameter κ

$$\mathrm{p} = \begin{bmatrix} \alpha_{11} & \alpha_{22} & \alpha_{33} & 0 & 0 & 0 \end{bmatrix} \tag{30}$$

$$\mathrm{P} = 2 \begin{bmatrix} * & -\alpha_{12} & -\alpha_{31} & 0 & 0 & 0 \\ -\alpha_{12} & ** & -\alpha_{23} & 0 & 0 & 0 \\ -\alpha_{31} & -\alpha_{23} & *** & 0 & 0 & 0 \\ 0 & 0 & 0 & 3\alpha_{44} & 0 & 0 \\ 0 & 0 & 0 & 0 & 3\alpha_{55} & 0 \\ 0 & 0 & 0 & 0 & 0 & 3\alpha_{66} \end{bmatrix},$$

$$* = \alpha_{31} + \alpha_{12},\ ** = \alpha_{23} + \alpha_{12},\ *** = \alpha_{31} + \alpha_{23} \tag{31}$$

with

$$\alpha_{ii} = \overline{\sigma}^2 \left(\frac{\overline{\sigma}_{iiC} - \overline{\sigma}_{iiT}}{\overline{\sigma}_{iiC}\overline{\sigma}_{iiT}} \right), \qquad i = 1,2,3 \tag{32}$$

$$\alpha_{ii} = \frac{\overline{\sigma}^2}{3\overline{\sigma}^2_{iiC}}, \qquad \begin{cases} i = 4,\ j = 2,\ k = 3 \\ i = 5,\ j = 3,\ k = 1 \\ i = 6,\ j = 1,\ k = 2 \end{cases} \tag{33}$$

$$\alpha_{ij} = \frac{\overline{\sigma}^2}{2} \left(\frac{1}{\overline{\sigma}_{iiC}\overline{\sigma}_{iiT}} + \frac{1}{\overline{\sigma}_{jjC}\overline{\sigma}_{jjT}} - \frac{1}{\overline{\sigma}_{kkC}\overline{\sigma}_{kkT}} \right), \qquad \begin{cases} i = 1,\ j = 2,\ k = 3 \\ i = 2,\ j = 3,\ k = 1 \\ i = 3,\ j = 1,\ k = 2 \end{cases} \tag{34}$$

In order to account for release of energy and redistribution of forces which caused the formation of a crack, a bilinear local softening model is adopted. It is proved as an efficient way of avoiding the mesh dependency of the results [11]. The additivity postulate of computational plasticity is used to formulate the rate form of the stress return algorithm. The integration of the flow rule in a finite step is then performed by the backward Euler method coupled with the Newton-Raphson iterative scheme, resulting in the following consistent tangent matrix D_{CT} [11]

$$\dot{\sigma}_j = \mathrm{D}_{CT}\dot{\epsilon}_j \tag{35}$$

$$\mathrm{D}_{CT} = \mathrm{Q}\left[\mathrm{I} - \frac{\mathrm{a}\mathrm{a}^T\mathrm{Q}}{\mathrm{B} + \mathrm{a}^T\mathrm{Q}\mathrm{a}}\right] \tag{36}$$

where

$$\mathrm{Q} = \mathrm{D}(\mathrm{I} + \Delta\lambda_j \mathrm{D}\mathrm{P})^{-1} \tag{37}$$

and a is the stress derivative of the yield function

$$\mathrm{a} = \frac{\partial\phi}{\partial\sigma_j} = \mathrm{P}\sigma_j + \mathrm{p} \tag{38}$$

and

$$\mathrm{B} = \frac{\partial\phi}{\partial\overline{\sigma}}\frac{\partial\overline{\sigma}}{\partial\kappa}\frac{\partial\kappa}{\partial\Delta\lambda_j} \tag{39}$$

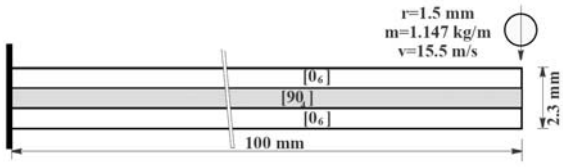

Figure 4. Geometry of composite impact problem.

(a) time=0.1 ms

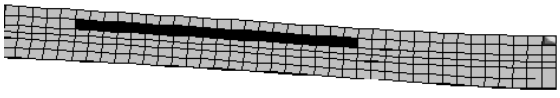

(b) time=0.6 ms

Figure 5. Delamination propagation (black region) on the deformed shape of the plate at times 0.1ms and 0.6 ms, respectively.

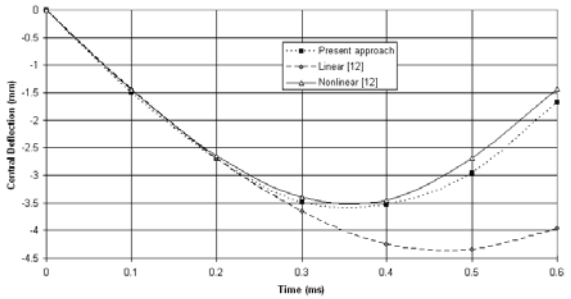

Figure 6. Displacement history of central point of the plate in comparison to [12].

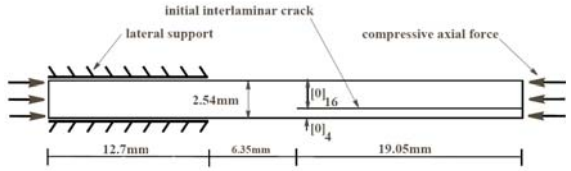

Figure 7. Geometry of an axially loaded composite panel with an initial interlaminar crack.

Using the consistent tangent matrix D_{CT} ensures the quadratic convergence rate for the stress update procedure at the Gauss point level and the overall solution.

The numerical procedure can be summarized as:

1. An explicit time integration scheme is adopted to determine displacements, velocities and accelerations for each time step. It will be followed by evaluation of strains at element levels.
2. The Hoffman elastoplastic material model is used to evaluate stress states.
3. Interlaminar stresses are determined using frictional contact algorithms (combined finite/discrete element method).
4. Hashin interlaminar criterion is adopted to check for occurrence of delamination and necessary stress updates.
5. Global and element matrices are updated.
6. Next impact load increment is applied and the procedure is repeated from step 1.

NUMERICAL SIMULATIONS

Delamination in a Composite Plate Subjectred to an Impact

A clamped $[0_6/90_4/0_6]$ composite beam, subjected to an impact by a cylindrical rigid object along its central line is considered (Figure 4). Composite material properties are defined in Table 1. Because of the symmetry, only half of the problem is modelled and only the delamination failure is investigated.

Table 1. Composite material properties.

E_{11}= 156 GPa	ν_{12}=0.228
E_{22}= 9.09 GPa	ν_{23}=0.4
G_{IC}=147 J/m^2	ρ= 1540 kg/m^2
G_{IIC}=526 J/m^2	
$Z_0 = 4MPa$	$R_0 = 2MPa$

Geubelle et al. [12] performed a full fracture analysis of the beam with matrix cracking by using 33180 LST and 23773 cohesive triangular elements. The present simulation is performed with the combined finite/discrete element method, showing more efficiency and reduction in computational efforts. Each layer is considered as a discrete body and is discretized by a finite element mesh. Interactions among discrete bodies (i.e. layers) are governed by fully nonlinear normal and frictional contact algorithms. Deformation and delamination patterns of the plate are shown in Figure 5 at times 0.1ms, 0.6 ms, respectively.

Displacement history of the central point of the plate has been shown in Figure 6, showing good agreement with the reference results obtained from nonlinear analysis [12].

Buckling of a Delaminated Composite Panel

This example is dedicated to the buckling behaviour of delaminated composite layers, previously studied by Progini et al.[13]. A panel, composed of $[0_{20}]$ composite layers with an initial crack between the $0_4/0_{16}$ layers, is subjected to incrementally increasing axial compressive loading until local and global buckling modes are generated in 0_4 and 0_{16} layers, respectively. (Figure 7 and Table 2).

Normal and frictional contact interaction laws have been considered for delaminated layers, while mixed mode criteria have been adopted for calculation of delamination propagation. An initial local deformation of the finite element model is depicted in Figure 8.

Figure 9 shows the predicted local and global buckling modes, while Figure 10 illustrates the load-displacement diagrams for two points A and B on $[0_4]$

Figure 8. Initial local deformation of the finite element model of the composite panel.

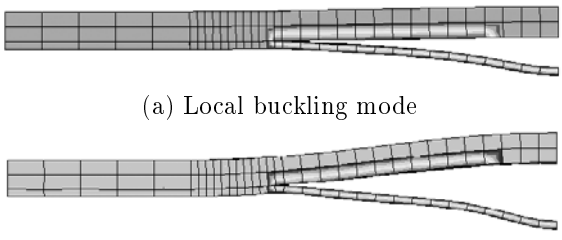

(a) Local buckling mode

(b) Global buckling mode

Figure 9. Deformed finite element mesh showing local and global buckling modes.

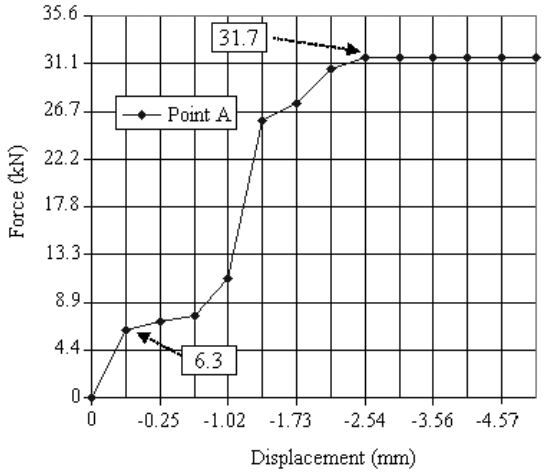

(a) point A

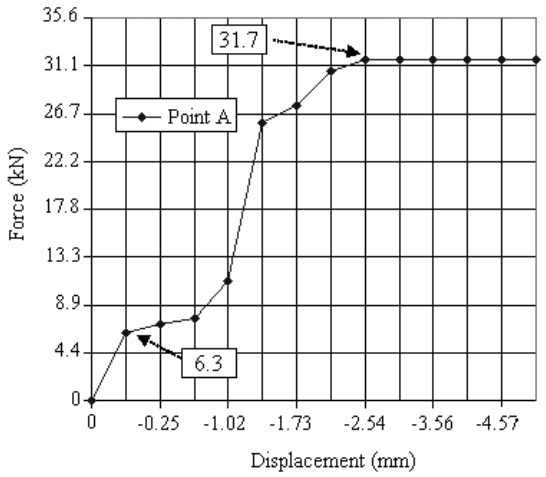

(b) point B

Figure 10. Load-displacement curves for points A and B, showing local and global buckling loads at 1410 and 7130 lbf, respectively.

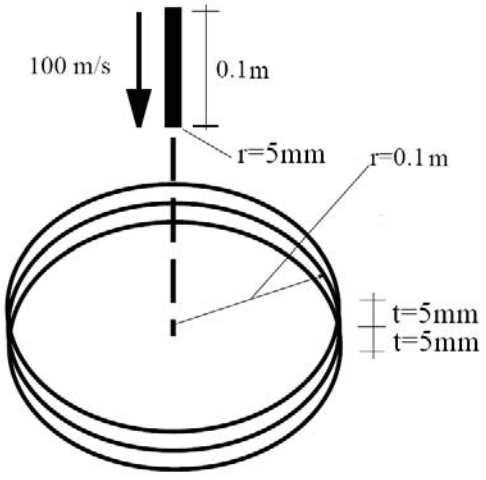

Figure 11. Geometry of the circular plate.

and $[0_{16}]$ layers, respectively. According to Figure 10, local buckling commenced at load 6.3 kN and global buckling occurred at load 31.7 kN, comparable to the results reported by Progini [13] at 5.8 kN and 34.8 kN, respectively.

Table 2. Material properties of composite panel [13]. (Original data were in lb-in units).

E_{11} = 139.2 GPa	ν_{12} = 0.29
E_{22}=9.72 GPa	ν_{12} = 0.29
E_{33} =9.72 GPa	ν_{12} = 0.29
G_{12} =5.58 GPa	G_{23} = 3.76 GPa
$\overline{\sigma}_{11T}$ =1510 MPa	$\overline{\sigma}_{11C}$ = 1590 MPa
$\overline{\sigma}_{22T}$ =45 MPa	$\overline{\sigma}_{22C}$ = 250 MPa
$\overline{\sigma}_{12S}$ = 107 MPa	
G_{IC} = 88 N/m	G_{IIC} = 88 N/m
$Z_0 = 4MPa$	$R_0 = 2MPa$

Table 3. Material properties.

Isotropic Plate	Projectile
$E = 152400\ MPa$	$E = 210000\ MPa$
$\nu = 0.35$	$\nu = 0.29$
$G = 4226\ MPa$	$G = 133000\ MPa$
$\rho = 1550 kg/m^3$	$\rho = 7860 kg/m^3$
$Z_0 = 4\ MPa$	
$R_0 = 4MPa$	

High Velocity Impact on a Circular Multi Layer Plate

This test is performed to illustrate the effects of various contact related parameters on the quality of the results for a 3D simulation of high velocity impact on a multi layer model. Similar numerical studies have to be performed for each independent simulation in order to properly set the associated contact interaction parameters.

A two layer circular composite plate subjected to an impact by a high velocity long rod is analyzed in different conditions (see Figure 11 and Table 3). The finite element model is depicted in Figure 12.

At first, the effect of hourglass control on the quality of the solution is investigated. The initial stable time step is $\Delta t = 0.1e-6$. Figure 13a illustrates an unstable solution that can be developed if no hourglass control is adopted.

In the next test, the penalty term is taken as $\alpha = 2e10$. According to Figure 13b, the rod quickly passes through the plate, and although it generates some internal stresses within the plate, the results are not reliable. Increasing the penalty term to $\alpha = 2e12$ leads to greatly improved results.

In another case, normal and tangential penalty parameters are set to different values of $\alpha_n = 2e12, 2e14$ and $\alpha_t = 2e10, 2e12, 2e14$. The two layers perform together and resist against the penetrating rod. The main source of error in this simulation is that the top layer deforms drastically (Figure 13c) and

causes the solution to be fatally terminated due to extensive hourglass instability (Figure 13d).

Finally, the best result is achieved by setting $\alpha_n = 2e14$, $\alpha_t = 2e14$ and $\Delta t = 0.1e-7$. The solution is acceptable for successive time steps until $t = 0.0004s$ (Figure 14) where the solution fails to converge due to very large deformation and distortion of the elements. It is not always an easy task to perform a full 3D contact delamination analysis due to several potential instability modes resulting from a large number of causes including layer separation, excessive penetration, spurious modes, distortion and hourglassing

Impact On a Concrete Beam Strengthened by CFRP

An impact experiment, performed by Jerome et al. (1997) [14] on a 3×3×30 in (7.62×7.62×76.2 cm) concrete beam (without internal steel reinforcement) and strengthened by a 3×30 inch three-ply CFRP panel, was analyzed to study the effects of debonding of the composite layer (FRP) from a different material. The measured dynamic drop loading curve versus time is shown in Table 4. Properties of concrete and CFRP panels are also given in Table 5.

Analysis was conducted in a plane stress state with adaptive triangular plane stress elements for both

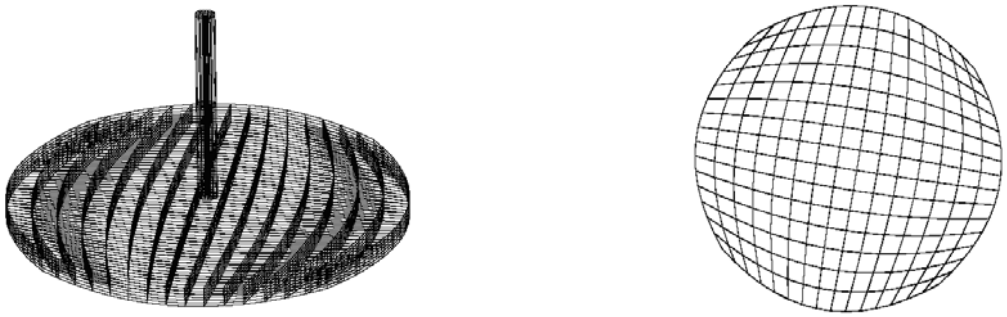

Figure 12. Finite element modelling of the circular plate from different view points.

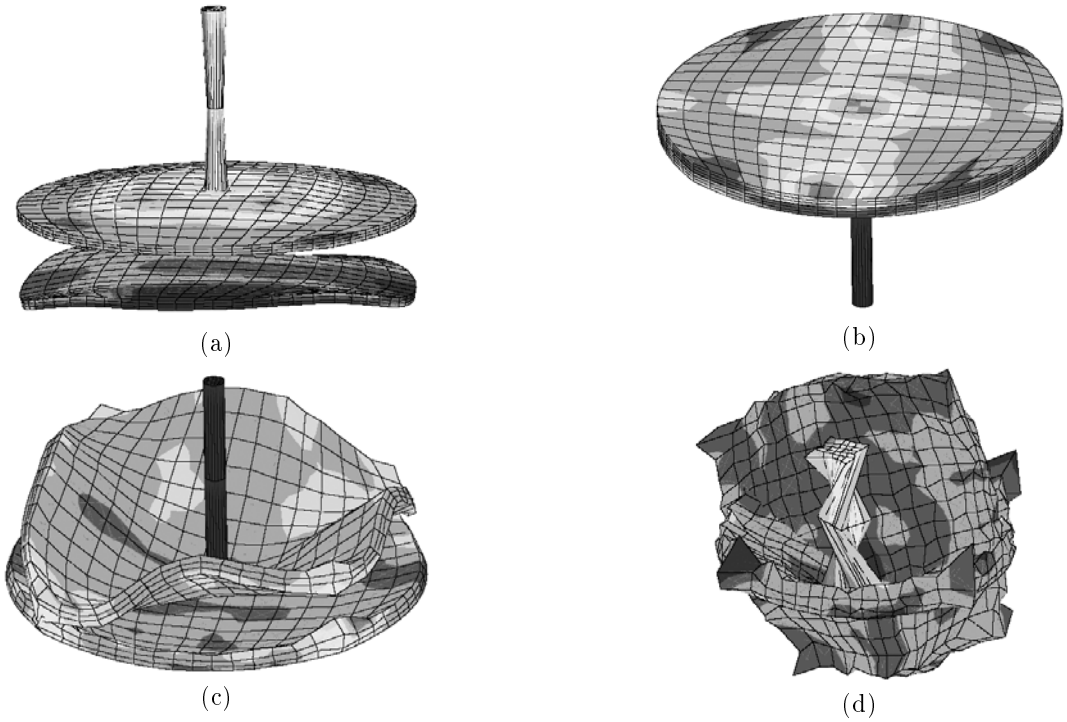

Figure 13. Instability modes; a) Layer separation and hourglass instability mode due to spurious modes. b) Large penetration of the rod has not created reasonable deformation in the circular plate. c) Large deformation of the top layer whilst acceptable deformation is generated for the bottom layer. d) Hourglassing and extensive distortion of the model.

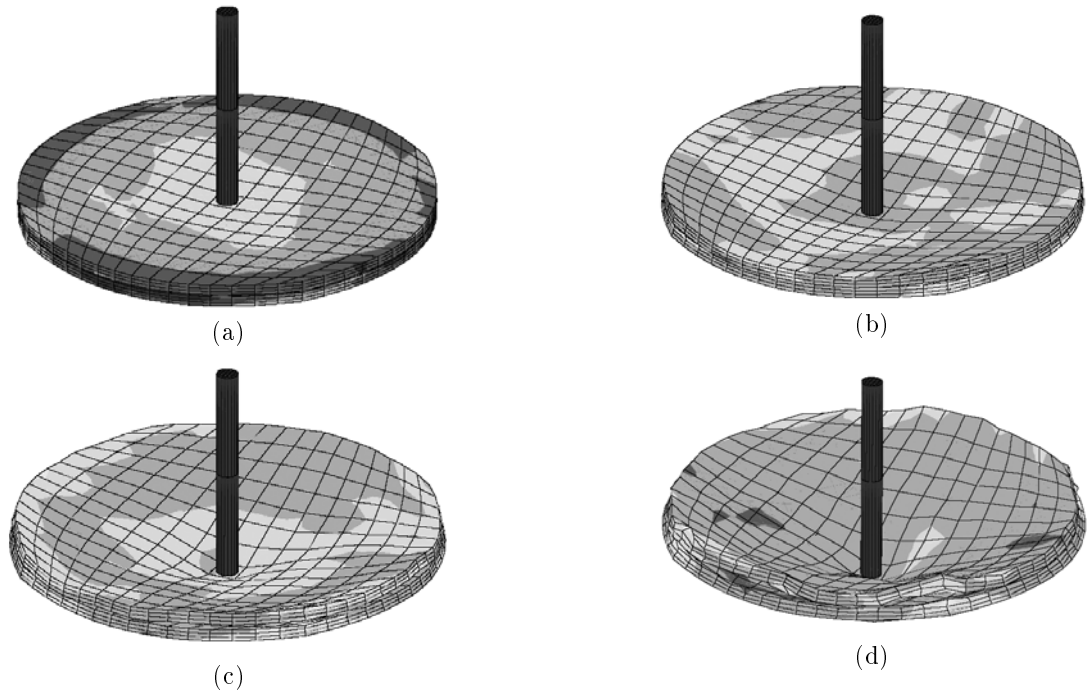

Figure 14. Deformed shape of the rod and plate at times a) 0.00005, b) 0.00015, c) 0.00025 and d) 0.00035 sec.

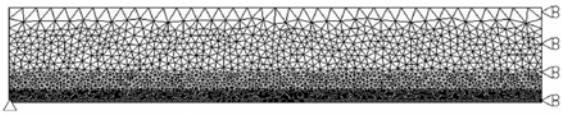

Figure 15. Finite element mesh and boundary conditions.

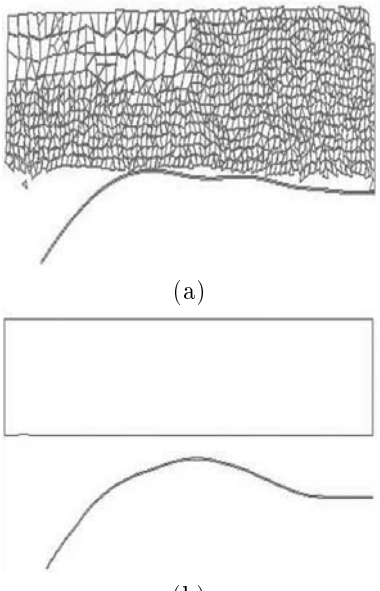

Figure 16. Unrealistic fracture (a) and delamination (b) predictions due to improper contact (interface) modelling.

the concrete beam and CFRP sheet. The size of these elements varied due to their distance from CFRP sheet; 0.01, 0.001 and 0.00025 m for elements adjacent to top of the beam, adjacent to CFRP, and CFRP itself, respectively. Because of the symmetry of loading and geometry only one half of the beam was modelled as depicted in Figure 15.

Unrealistic deformation and fracture modes may be triggered if any of several parameters affecting the results such as contact related parameters, bonding/interface variables, size of the timestep, fracture properties and material related data are improperly set (Figure 16). Jerome [14] reported that flexural cracks started to occurr between 400-500 μs and, ran to the upper surface of the beam by 600 μs, which is in a close agreement with results of the performed simulation (Figure 17).

Test indicated occurrence of a crack initiation on the bottom centre of the beam at about 430 μs. The results show that flexural cracks were propagated at

Table 4. Load (kN)-time(ms) curve [14].

time	load	time	load	time	Load
0.0	0.0	0.8	1.1	2.1	15.8
0.2	31.1	1.0	1.8	2.4	13.3
0.3	35.6	1.2	8.9	2.6	13.3
0.4	31.1	1.4	14.2	2.9	18.2
0.5	28.9	1.6	8.9	3.0	17.8
0.6	4.4	1.8	11.1	3.2	11.6
0.7	0.0	2.0	15.1	3.4	6.7

Table 5. Concrete and CFRP material properties.

Concrete		CFRP	
E_0	24000 MPa	$\overline{\sigma}_{0T}$	2206.9 MPa
ν	0.2	$\overline{\sigma}_{90T}$	137.9 GPa
f_t	4.35 MPa	fibre volume	60 %
f_c	46.4 MPa	3-ply thick.	0.4953 mm
σ_t	39.5 MPa		
ρ	1892.7 kg/m^3	ρ	1577.2 kg/m^3
G_f	0.5 N/mm		
Z_0	4 MPa	R_0	4 MPa

the bottom part of mid span at 460μs. These flexural cracks started to propagate from two distinct origins very close to mid span. Later, these cracks started to develop, and reach the upper surface of the beam in time interval of 460 μs to 750 μs[14].

On the other hand, the present numerical approach predicts distinct cracks to attach to each other at 0.00113s. Later, at 0.00127s some signs of delamination are observed at the bottom of the beam, developing gradually at 0.00132s. At 0.00165s microcracks start to develop from about mid height of the beam toward the left side. They reach the bottom of the beam, creating a complete flexural cracking beside microcracks at 0.00171s. It is notable that these cracks stop exactly at the same location where delamination of CFRP stops.

1200 and 630 8-noded cubic elements were used for 3D modelling of the FRP sheet and concrete beam, respectively. Similar to 2D simulation, the size of elements were gradually increased for the concrete beam by their distance from the bottom of the beam by an increasing ratio of 0.7^{-1}. A node to face contact approach was adopted for modelling the adhesive layer and the contact of the adjacent elements. Again, improper setting of the interface contact related parameters produces unrealistic delamination patterns as depicted in Figure 18. Figure 19 shows the debonded region of CFRP sheet from mid span at 470 μs and 750 μs.

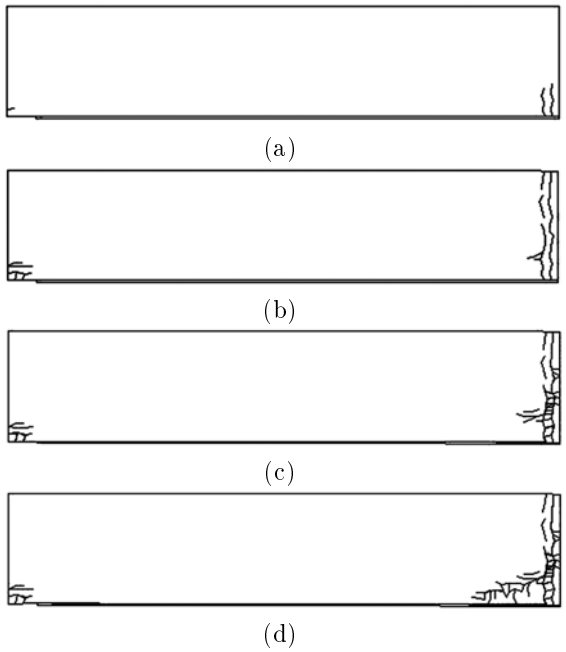

Figure 17. Cracking Pattern at time steps (a).00046s, (b).00075s, (c).000165s and (d).00174s.

Delamination of CFRP sheet from the concrete beam was approximately started at 470 μs in the middle of the beam and propagated toward the support. At 750 μs about one fifth of the total length of FRP sheet was debonded from the bottom of the beam as illustrated in Figures 19.

Various displacement history curves at mid span of the beam, computed in different 2D and 3D simulations, were compared to the displacement history resulting from the experimental tests as depicted in Figure 20. The existing large differences of no fracture results can be attributed to the fact that the simulated beam has more stiffness than the experimental beam, which is a consequence of elastic behavior of concrete in tensile regime without any tensile fracture.

CONCLUSIONS

A contact based delamination control has been developed and implemented within a combined finite/discrete element method. It has resulted in a reliable and efficient approach to delamination and

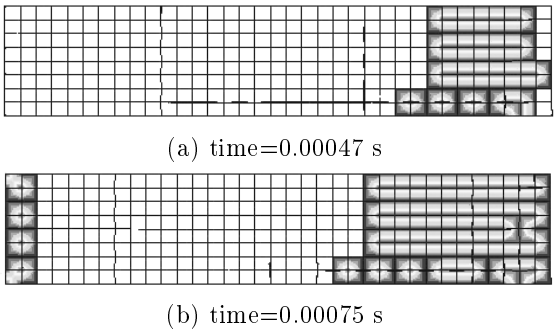

Figure 18. Unrealistic 3D interface debonding patterns.

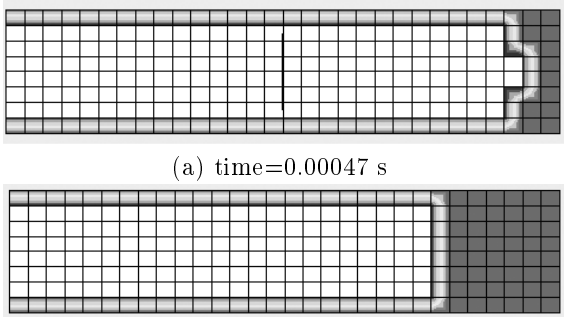

Figure 19. Delamination growth at different time steps.

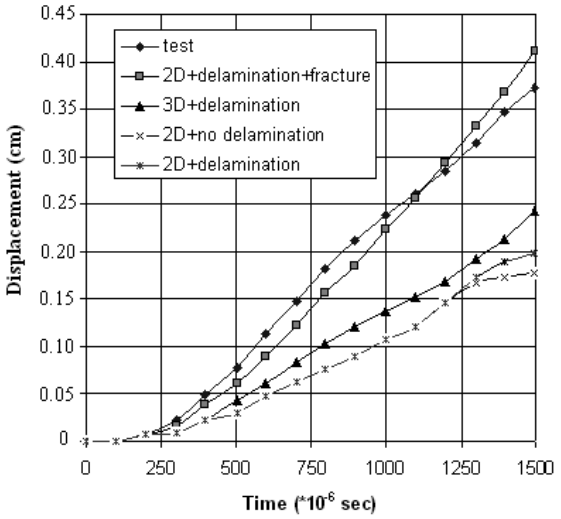

Figure 20. Comparison of mid point displacement vs. time for different solutions.

fracture analysis of composites subjected to high velocity projectiles. Initiation and propagation of cracks have been considered using a bilinear strain-softening model. The penalty method has been employed to impose impenetrability and post-debonding behaviors of plies as well as post-cracking of individual layers. Numerical tests have demonstrated the power of the algorithm for numerical simulation of impact loading on composite structures. The method has performed well for similar applications such as dynamic behavior of concrete structures strengthened by FRP composites.

REFERENCES

1. Rowlands, R.E., "Strength (Failure) Theories and Their Experimental Correlation", *Handbook of Composites*, Failure Mechanics of Composites, Elsevier, **3**, PP 71-125(1985).
2. Chen, W.H. and Yang, S.H., "Multilayer Hybrid-Stress Finite Element Analysis of Composite Laminates with Delamination Cracks Origination from Transverse Cracking", *Engineering Fracture Mechanics*, **54**(5), PP 713-729(1996).
3. Kwon, Y.H. and Aygunes, H., "Dynamic Finite Element Analysis of Laminated Beams with Delamination Cracks Using Contact-Impact Conditions", *Computers & Structures*, **58**(6), PP 1161-1169(1996).
4. Mohammadi, S. and Owen, D.R.J. and Peric, D., "A Combined Finite/Discrete Element Algorithm for Delamination Analysis of Composites", *Finite Elements in Analysis and Design*, **28**, PP 321-336(1998).
5. Hashagen, F. and de Borst, R., "Numerical Assessment of Delamination in Fibre Metal Laminates", *Computer Methods in Applied Mechanics and Engineering*, **185**, PP 141-159(2000).
6. Sprenger, W. and Gruttmann, F. and Wagner, W., "Delamination Growth Analysis in Laminated Structures with Continuum-Based 3D-Shell Elements and a Viscoplastic Softening Model", *Computer Methods in Applied Mechanics and Engineering*, **185**, PP 123-139(2000).
7. Mohammadi, S., *Discontinuum Mechanics Using Finite and Discrete Elements*, WIT Press, (2003).
8. Mohammadi, S. and Forouzan-sepehr, S. and Asadollahi, A., "Contact Based Delamination and Fracture Analysis of Composites", *Thin-Walled Structures*, **40**, PP 595-609(2002).
9. Schellekens, J.C.J., "Computational Strategies for Composite Structures", Ph.D. Thesis, Delft University of Technology(1992).
10. Mohammadi, S. and Forouzan-sepehr, S., "3D Adaptive Multi Fracture Analysis of Composites Materials Science Forum", PP 440-441, 145-152(2003).
11. Mohammadi, S. and Mousavi-Khandan, A.A., "Simulation of Bond Failure in RC Beams Strengthened with FRP Sheets Subjected to Dynamic/Impact Loadings", *Proceedings of International Symposium on Bond Behaviour of FRP in Structures*, (2005).
12. Geubelle, P.H. and Baylor, J.S., "Impact-Induced Delamination of Composites: a 2D Simulation", *Composites Part B 29B*, PP 589-602(1998).
13. Progini, P. and Riccio, A. and Scaramuzzino, F., "Influence of Delamination Growth and Contact Phenomena on the Compressive Behavior of Composite Panels", *Journal of Composite Materials*, **33**(15), PP 1433-1465(1999).
14. Jerome, D.M. and Ross, C.A. , "Simulation of the Dynamic Response of Concrete Beams Externally Reinforced with Carbon-Fiber Reinforced Plastic", *Computers and structures*, **64**(5/6), PP 1129-53(1997).